SAND2012-3076 C

SAND2012-3076C

Electromagnetic eXtended Finite Elements for Accurate Resolution of Multi-Material Cells

Christopher M. Siefert, Thomas E. Voth, and Pavel B. Bochev

Sandia National Laboratories, Albuquerque, NM
csiefer@sandia.gov, tevoth@sandia.gov pbboche@sandia.gov

Sandia National Laboratories is a multi-program laboratory managed and operated by Sandia Corporation, a wholly owned subsidiary of Lockheed Martin Corporation, for the U.S. Department of Energy's National Nuclear Security Administration under contract DE-AC04-94AL85000.

Abstract

Surface effects are critical to the accurate simulation of electromagnetics (EM) as current tends to concentrate near material surfaces. Applications of interest to Sandia and ARL operate in a large deformation, large vorticity regime, where body-fitted meshes are impractical and multimaterial elements are the only feasible option. Unlike their hydrodynamic counterparts, mixture models for EM-related properties are often quite poor, which can significantly compromise the accuracy of the simulation in this very important surface region.

Highly-accurate edge-based (compatible) discretizations [6] form the basis for ALEGRA-MHD simulations, as they correctly respect the underlying physics. Unfortunately, there is no edge-based method that allows for resolution of sub-element material interfaces. One approach to this problem is to extend the ideas of the eXtended Finite Element Method (XFEM) [20] to edge-based discretizations. Although the XFEM has been applied to nodal and element-based discretizations, only recently has preliminary work begun for these edge-based schemes [17].

We will present an outline of how the XFEM method can be extended to EM phenomena, noting the research questions which need to be addressed before EM-XFEM can be used as a production capability. These include allowing electric field discontinuities normal (but not tangential) to material boundaries (as required by the physics) and the discrete computation of divergence-free updates to the (face-element) magnetic field to allow the satisfaction of Gauss' law for magnetism.

I Introduction

Surface effects are often important to understanding electromagnetic phenomena, especially those that are transient in nature, for the simple reason that current tends to concentrate on material surfaces and interfaces. When computationally modeling EM phenomena, accurate resolution of material interfaces can often make the difference between a correct answer and an incorrect one. In the context finite element method (FEM), the simplest way to deal with this is to create a body-fitted mesh with sufficient resolution and have it move with the material when the material moves (the Lagrangian approach). For problems in the small deformation regime, this approach works very well. Unfortunately, many problems of interest to Sandia and the Army do not fall into this regime. They routinely included large material deformation and phenomena like impact and fragmentation. For these problems, body-fitted meshes are untenable, leaving non-moving (Eulerian) meshes as the alternative. This means developing a systematic treatment for multimaterial elements.

One problem of interest to Sandia is the magnetic acceleration flyer plates [18]. In this application, small metal plates are accelerated magnetically to high velocity so that shock wave experiments can be performed. Figure 1 shows a diagram of a typical flyer plate experiment, taken from the ALEGRA-MHD

training course [11]. The Lorentz force pushes the flyer plate upward towards the target. Measurements of the flyer and shock waves velocities can then be used to obtain values for the material's equation of state (EOS) along the shock Hugoniot. We are interested computer simulation of this process, because it allows us to experiment with different current pulses in order to minimize joule heating and shock formation before impact, to maintain the validity of the experiment.

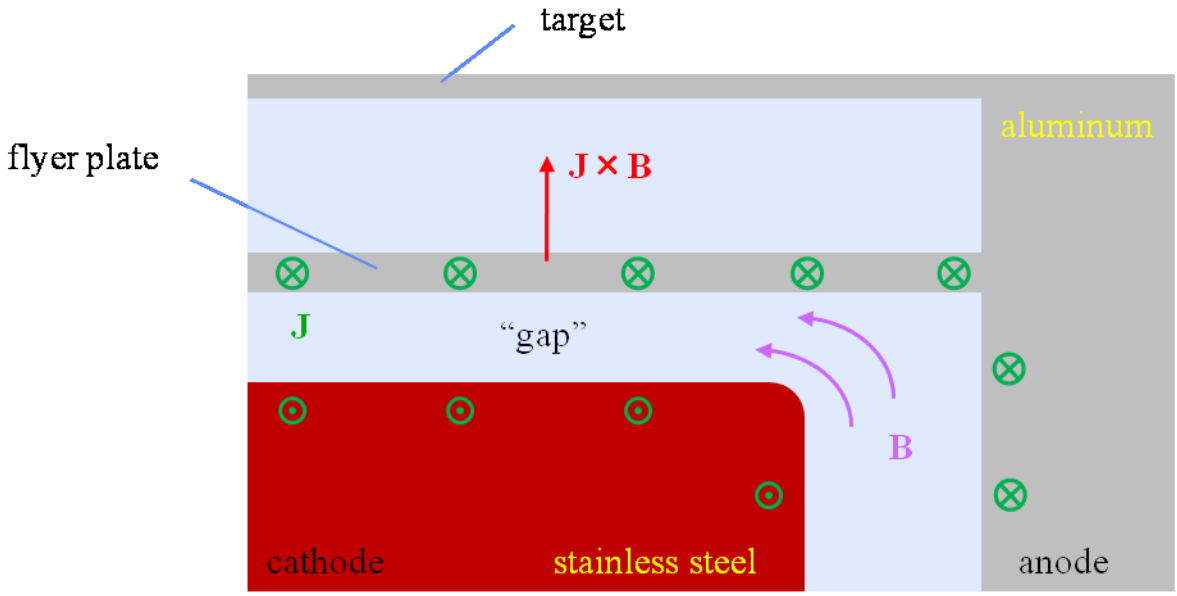

Figure 1: Diagram of a magnetic flyer plate experiment showing the flyer plate, target, anode, cathode and the direction of the electric and magnetic fields

Figure 2 shows a sample flyer plate calculation from the ALEGRA-MHD training course [11] at three different times. In this problem, current is driven through the center light blue strip and the Lorentz forces accelerate it towards the target at the top of the figure. The white lines represent logarithmically spaced isosurfaces of the current density. Note that at 3 μs, the current is highly concentrated near the edges of the flyer plate. Since the flyer hits the target a mere 0.2 μs later, we cannot handle this problem in a Lagrangian fashion and instead have to resort to an Eulerian approach in Figure 2.

Another problem of interest is simulation of magnetic flux compression generators [9, 12]. In this application, some external force (usually from a chemical explosive) is used to drive two conducting surfaces into contact. The motion of those conductors concentrates magnetic energy in the remaining gap between the two contacts. Figure 3 shows a sample flux compression generator experiment. In this picture the red explosive will detonate, pushing the right wire towards the left one, compressing the magnetic field between the wires. Eventually the two wires will contact, isolating the magnetic field between the wires at the bottom part of the loop.

These devices are of interest in applications where large magnetic fields are needed. Given the "one-shot" nature of the flux compression generator, computer simulation can significantly reduce the number (and expense) of an experimental program. Figure 4 shows a simulation flux compression at three different times [9]. Material density is shown by color. At time $t = 1$ μs, we see a loop of (red) material which is carrying a current, and an explosive to the right. When the explosive begins to expand, the right part of the loop is pushed leftward, resulting in contact in Figure 4(c). Like the magnetic flyer case, we note the collapse of the region between the conductors as they move towards contact, rendering a Lagrangian mesh untenable, again forcing us to an Eulerian, multimaterial element approach. In this problem, the edge artifacts on the moving conductor are due to partially filled multimaterial cells.

In the hydrodynamics community, mixture models for multimaterial elements have had a long and successful history [1, 2, 10]. However, mixture models for magnetic phenomena have been studied only in

(a) Flyer plate at $t = 0\ \mu s$.

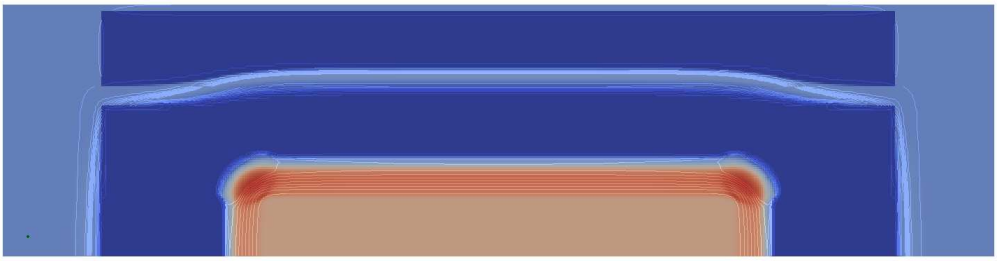

(b) Flyer plate at $t = 3\ \mu s$.

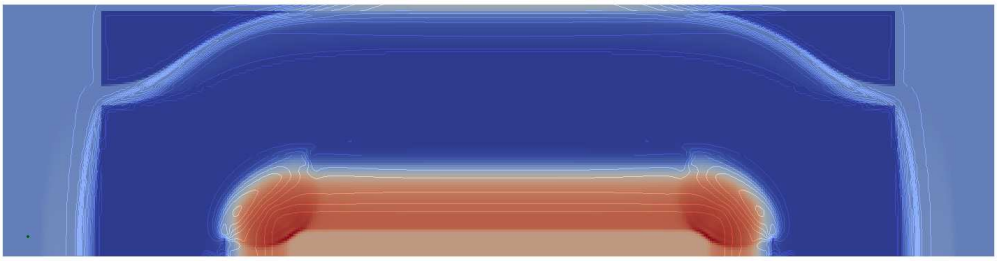

(c) Flyer plate at $t = 3.2\ \mu s$.

Figure 2: Sample flyer plate calculation at 0, 3 and 3.2 microseconds. Density is shown by color. White lines represent isosurfaces of the current density.

relatively focused areas, like laminated iron cores [13], laminated shields [27] or dielectric mixtures [24]. Using an *ad hoc* model can often lead to loss spatial of accuracy relative to a discretization which correctly resolve the material interface.

Given the relative immaturity of magnetic mixture models, we choose to take an alternative approach to multimaterial elements, based on the extended finite element method (XFEM). The simplest way to explain the XFEM [8, 20] is that this method adds basis functions (and potentially constraints) to the existing FEM basis in order to resolve material discontinuities. In this paper, we extend the XFEM to magnetic discretizations, and demonstrate that we achieve accuracy near that of a body-fitted Lagrangian mesh on several model problems. In Section II, we review the edge-based discretizations commonly used in MHD codes like ALEGRA [22]. We likewise review the XFEM in Section III, followed with development of magnetic XFEM in Section IV. We provided numerical examples of our proposed technique in Section V and conclude in Section VI.

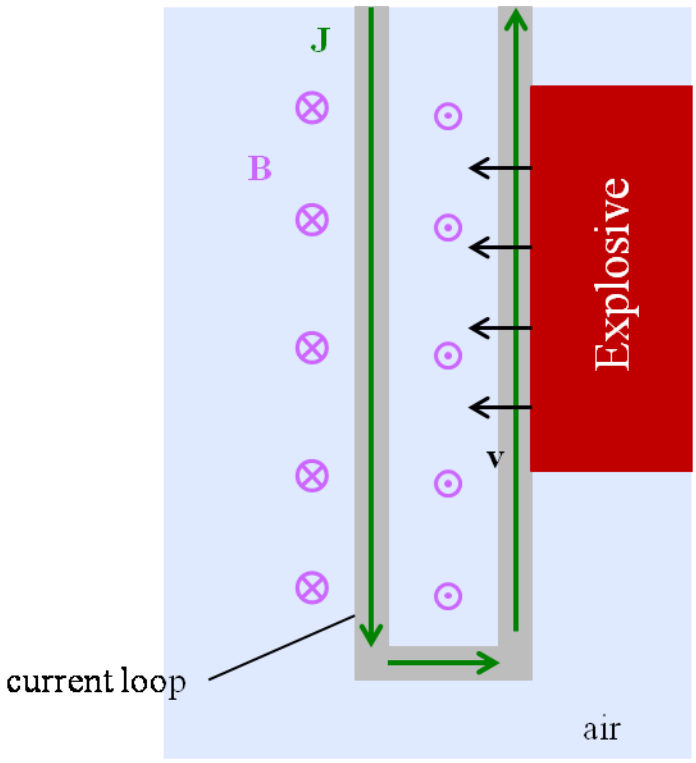

Figure 3: Diagram of a magnetic flux compression generator experiment showing current carrying loop, the explosive, electric and magnetic fields

II Edge Element Discretizations for Magnetics

After neglecting the displacement currents, polarization and magnetization, the Maxwell's equations simplify to the parabolic eddy current equations

$$\nabla \cdot \mathbf{B} = 0, \tag{1}$$

$$\nabla \times \frac{\mathbf{B}}{\mu} = \mathbf{J}, \tag{2}$$

$$\nabla \times \mathbf{E} = -\frac{\partial \mathbf{B}}{\partial t}, \tag{3}$$

$$\mathbf{J} = \sigma \mathbf{E}, \tag{4}$$

where $\mathbf{B}$ is the magnetic flux density, $\mathbf{E}$ the electric field, $\mathbf{J}$ the current density, σ conductivity and μ permeability.

To approximate the eddy current equations we write the Ampere law in weak form and use the backward Euler rule to discretize the time derivative in the Faraday's law

$$\int_\Omega \frac{\mathbf{B}}{\mu} \cdot \nabla \times \widehat{\mathbf{E}}\, d\Omega + \int_\Gamma (\mathbf{n} \times \mathbf{H}_b) \cdot \widehat{\mathbf{E}}\, d\Gamma = \int_\Omega \sigma \mathbf{E} \cdot \widehat{\mathbf{E}}\, d\Omega, \tag{5}$$

$$\frac{\mathbf{B}^{n+1} - \mathbf{B}^n}{\Delta t} + \nabla \times \mathbf{E} = 0, \tag{6}$$

Substituting (6) into (5) and rearranging terms yields the semidiscrete in time eddy current equation in terms of the electric field only:

$$\int_\Omega \sigma \mathbf{E} \cdot \widehat{\mathbf{E}}\, d\Omega + \Delta t\, (\nabla \times \mathbf{E}) \cdot \nabla \times \widehat{\mathbf{E}}\, d\Omega = \int_\Omega \mu^{-1} \mathbf{B}^n \cdot \nabla \times \widehat{\mathbf{E}} + \int_\Gamma (\mathbf{n} \times \mathbf{H}_b) \cdot \widehat{\mathbf{E}}\, d\Gamma, \tag{7}$$

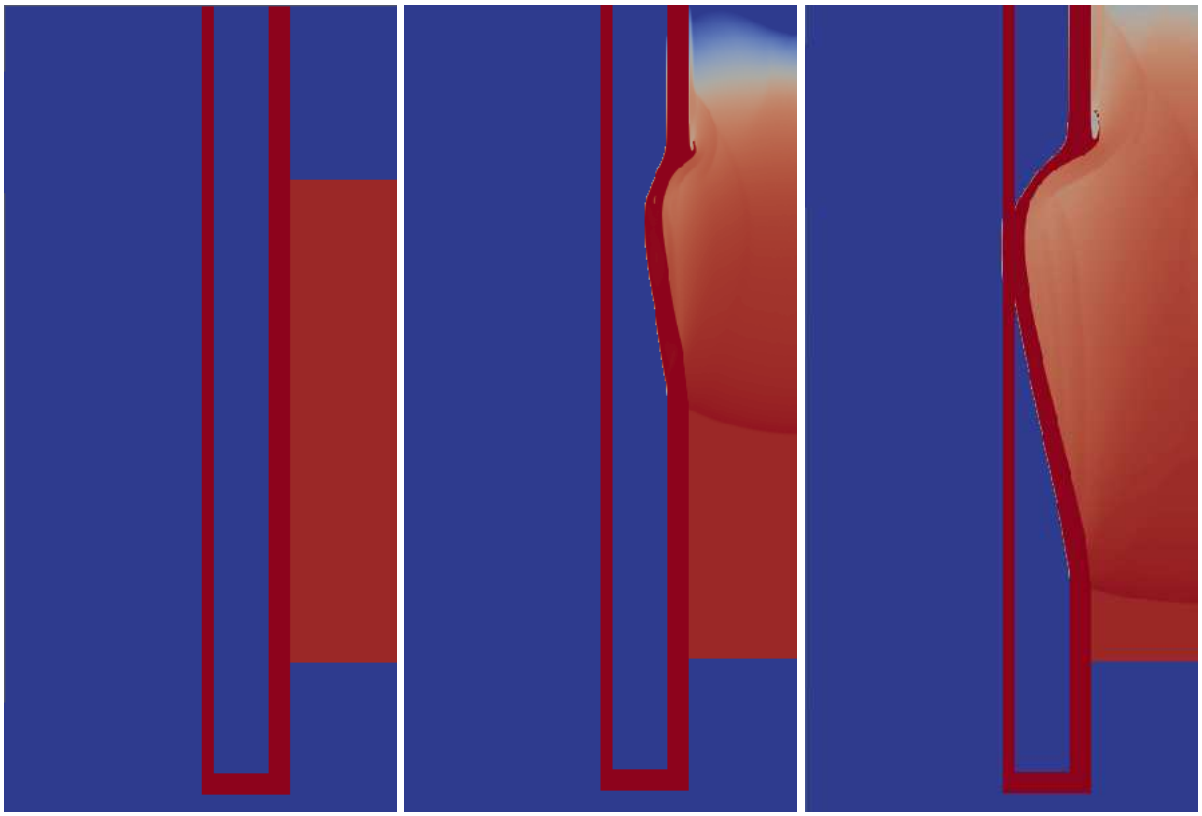

(a) Compression generator at $t = 1\ \mu s$. (b) Compression generator at $t = 10\ \mu s$. (c) Compression generator at $t = 15\ \mu s$.

Figure 4: Sample magnetic flux compression generator calculation at 1, 10 and 15 microseconds. Density is shown by color.

To discretize (7) in space we use the lowest-order Nedelec edge element [4, 5, 25]. Assuming that $\mathbf{E}$ is the edge element solution, we can compute the magnetic flux density from the semidiscrete in time Farady's law (6).

Figure 5 shows an example of a triangle with oriented edges. With this numbering, we can write the associated basis functions in physical space as

$$W_1(x,y) = \frac{1}{2A}\left(\begin{bmatrix} -y \\ x \end{bmatrix} + \begin{bmatrix} y_3 \\ -x_3 \end{bmatrix}\right), \tag{8}$$

$$W_2(x,y) = \frac{1}{2A}\left(\begin{bmatrix} -y \\ x \end{bmatrix} + \begin{bmatrix} y_1 \\ -x_1 \end{bmatrix}\right), \tag{9}$$

$$W_3(x,y) = \frac{1}{2A}\left(\begin{bmatrix} -y \\ x \end{bmatrix} + \begin{bmatrix} y_2 \\ -x_2 \end{bmatrix}\right), \tag{10}$$

where W_i is the basis function associated with edge i, and A is the signed area of the element.

The special structure of the edge element basis functions (8)–(9) allow us to define a discrete curl operator which maps fields on edges to fluxes through faces. This operator is merely the appropriately signed sum of the coefficients of the edge bases around the face of the element (think of it as a discrete line integral). For the element in Figure 5, if we want the curl pointing out of the page, this reduces to a sum of the coefficients of the edge bases (the edges are all pointing in the same direction as you walk the element counterclockwise). Via the (backward Euler time discretized) Faraday's law, this allows us to directly update $\mathbf{B}$ after each timestep. But since this discrete curl discretely satisfies the relation $\nabla \cdot \nabla \times = 0$, $\mathbf{B}$ then satisfies Gauss' law for magnetism ($\nabla \cdot \mathbf{B} = 0$) discretely. This property is one key reason why edge element discretizations work

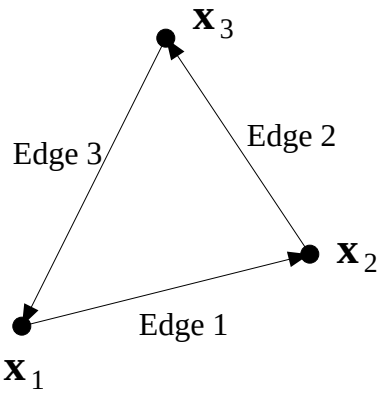

Figure 5: Triangular finite element with oriented edges.

so well for Maxwell's equations.

The second key property of edge elements, which makes them particularly well-suited for electromagnetics problems, is their ability to correctly represent the physical behavior of the electric field along material interfaces, assuming the mesh is fitted to the interface. Concretely, if material conductivity experiences a jump across an interface then so does the *normal* component of **E**, while its tangential component stays continuous. Approximation of the electric field by nodal elements, which are continuous across interfaces, does not posses this property and may lead to unphysical solutions.

III Extended Finite Elements (XFEM)

The eXtended Finite Element method (XFEM) was initially devised to model crack propagation in a mesh-independent fashion (cf. [8, 20]). It has since been expanded to a range of applications including two-phase fluid flow [7], simulation of hydrogels [15] and dislocation dynamics [21], among others.

The idea behind the XFEM is that a function can be represented as a combination of standard Finite Element Basis functions plus an enrichment term,

$$u^h(x,y) = \sum_I u_I^0 N_I(x,y) + \sum_\alpha \sum_I u_I^\alpha N_I(x,y) H_\alpha(x,y) \tag{11}$$

via the Partition of Unity framework [8, 19]. In (11) the $H_\alpha(x)$ is the "enrichment" function. A number of different functions have been used for $H(x)$ including both continuous and discontinuous functions depending on the application at hand. Indeed, quite complicated functions have been used in crack-tip and dislocation dynamics modeling where complex local features need be captured by the enrichment [20, 21].

Here H_α is assumed to be a Heaviside (or "indicator") function (i.e. one that takes on a value of one in regions where material α is present and zero elsewhere). An advantage of this choice is that it allows discontinuties in, for example, velocity field, as required when two materials slide relative to one another.

Because the first term on the right-hand-side of (11) can be reproduced with appropriate coefficients in the second right-hand-side terms it is dropped leaving only the terms multiplied by the indicator functions. As an example,

$$u^h(x,y) = \sum_I u_I^A N_I(x,y) H_A(x,y) + \sum_I u_I^B N_I(x,y) H_B(x,y) \tag{12}$$

for a two-material (materials A and B) problem. As a result, the response of the two materials may be represented as the sum of two (independent) elements. This approach was suggested independently by both Hansbo and Hansbo [14] and Song et al. [23] and forms the foundation of the ALEGRA solid mechanics XFEM approach [26].

IV Magnetic XFEM

We now consider employing tied Heaviside enrichment to edge element basis functions to develop a electromagnetic XFEM (EM-XFEM) capability. Since we wish to guarantee tangential continuity across a cut, we need two key properties. The first is an inherent property of d-simplices (e.g. triangles and tetrahedra) while the second is a property of lowest-order edge elements.

Property 1 *Straight lines in physical space map to straight lines in reference space on d-simplices (e.g. triangles and tetrahedra).*

Property 2 *Take a arbitrary triangle and a line. For a d-simplex, all lowest order edge basis functions have a constant tangential component on the line.*

The first property is a consequence of the Jacobian of a simplicial element being constant. The second property follows from (B.22) in [3] which states that edge basis functions can be written in the form $a+\mathbf{x}\times b$. In 2D the cross product in this result is defined as $\mathbf{u}\times p = (pu_2)\mathbf{i} - (pu_1)\mathbf{j}$. Combining Properties 1 and 2 allows us to guarantee tangential continuity everywhere along an XFEM cut with a single Lagrange multiplier constraint (tying the field anywhere is equivalent to tying it along the entire cut). In the case of quads or hexes, the first property only holds on an orthogonal mesh and the second only holds if the cut is orthogonal to the quad or hex. In these cases, tying the integral over the cut line is possible, but it will not guarantee tangential continuity everywhere along the cut. For this reason, we believe simplicial elements should be more robust for use with EM-XFEM

Figure 6 shows the two scenarios for cutting 2D triangles, with the cuts shown in red. Cut configuration #1 involves a cut which intersects a vertex and the opposite edge. Cut configuration #2 involves a cut between two edges. In this configuration, we add an additional (blue) cut which intersects a vertex of the quadrilateral portion of the element. We have the choice of two different blue cuts (one reaching $\mathbf{x}_1$ and the other reaching $\mathbf{x}_2$), so we choose the one which has the larger minimum angle. We need to add the additional (blue) cut in the second case to ensure that we have sufficient degrees of freedom to both span the appropriate space and maintain tangential continuity.

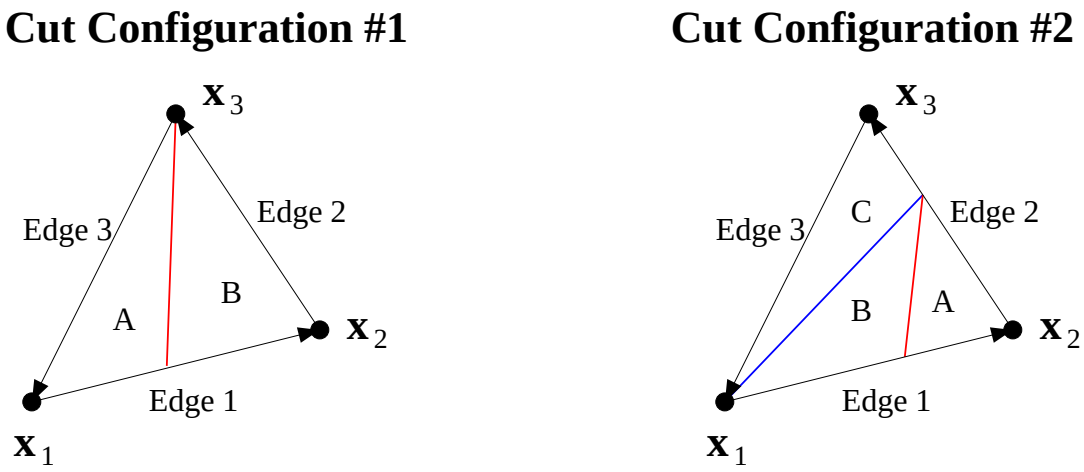

Figure 6: The two cut scenarios for 2D triangles. The red line represents the XFEM cut, a blue line represents an additional cut added to guarantee solution accuracy. Sub-elements are labeled with letters to describe regions over which Heaviside functions are non-zero.

We now define the Heaviside functions,

$$H_X(x,y) = \begin{cases} 1 & (x,y) \text{ in region X.} \\ 0 & (x,y) \text{ not in region X.} \end{cases} \tag{13}$$

for $X = A, B$ in configuration #1 and $X = A, B, C$ in configuration #2. For configuration #1 we now have the basis $\{H_A W_1, H_A W_2, H_A W_3, H_B W_1, H_B W_2, H_B W_3\}$, with the configuration #2 also adding $H_C W_i$, for $i = 1, 2, 3$. This results in functions which have non-zero value only in one of the two (or three) sub-element.

Having constructed the enriched basis functions, we now consider the tying. As we have shown above, we can constrain the tangential components of the field match at any point and will ensure they match everywhere on the cut line. We choose to constrain at the center of the cut. Let this point be $\mathbf{x}_c$ and the tangent to the cut be t. Then we can write our constraint for configuration #1 as

$$\sum_i E_{Ai} W_i(\mathbf{x}_c) \cdot t = \sum_i E_{Bi} W_i(\mathbf{x}_c) \cdot t, \tag{14}$$

where the E_i's represent the solution components corresponding to the basis functions on each side of the cut. For configuration #2, we need a second constraint for the blue cut. The constrained Lagrange multiplier equations from Heaviside enrichment are then added to the original linear system which results in an indefinite Karush-Kuhn-Tucker (KKT) system, which must then be solved at each timestep.

V Example

We begin by presenting a simple quasi-one-dimensional problem as illustrated in Fig. (7) to demonstrate the efficacy of the magnetic XFEM approach. For this example we made several simplifying assumptions for our analysis including i) that the mesh is quasi-one-dimensional and ii) that the cut-line is vertical and iii) that the element is not skewed (cf. Figure 7). Specifically, we have a vertical *cut-line* which aligns with the edges of the cut (rectangular) element. As indicated earlier we used Lagrange multipliers to enforce continuity in the tangential component of **E** along the cut. The assumptions above require that we use a rectangular edge element rather than the triangle described earlier. Details of the rectangular element may be found elsewhere (cf. [16]).

Solution convergence of the electric field at the cut as a function of mesh refinement shown in Fig. (8) for the EM-XFEM formulation. Also shown are convergence rates for body-fit FEM meshes (the cut is at an element boundary) and non-conforming FEM (the cut is internal to an element). From the figure it is clear that the EM-XFEM approach produces rates of convergence equal to that of the body-fit FEM problem. Lowest order edge elements are generally first order accurate, but under certain circumstances, such as orthogonal meshes with orthogonal material boundaries, we can expect second order accuracy, which is what we see from both the body-fit FEM and EM-XFEM solutions. Perhaps surprisingly the EM-XFEM result shows slightly lower error than the body-fitted result. The non-conforming FEM result show significantly reduced rates of convergence and greater error over the range of discretizations examined.

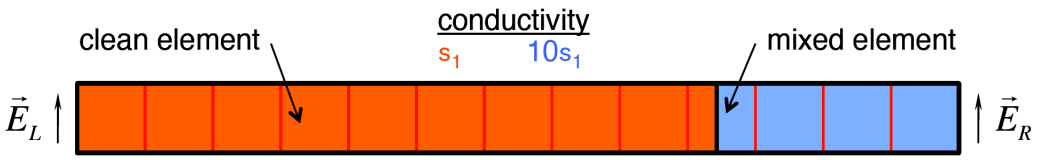

Figure 7: Quasi-one-dimensional problem specification and mesh.

VI Conclusions and Future Work

As noted previously, surface effects are often critical to the accurate simulation of EM phenomena as current tends to concentrate near material surfaces. The magnetic flyer plate and flux compression generator problems both illustrate problems where surface effects are critical, but where Lagrangian moving-mesh approaches are impractical. Following the XFEM methodology we developed a Lagrange multiplied tied Heaviside enrichment which is appropriate for lowest order edge element discretizations. We explained some of the theoretical underpinnings behind the method and demonstrated the recovery of the convergence rate of

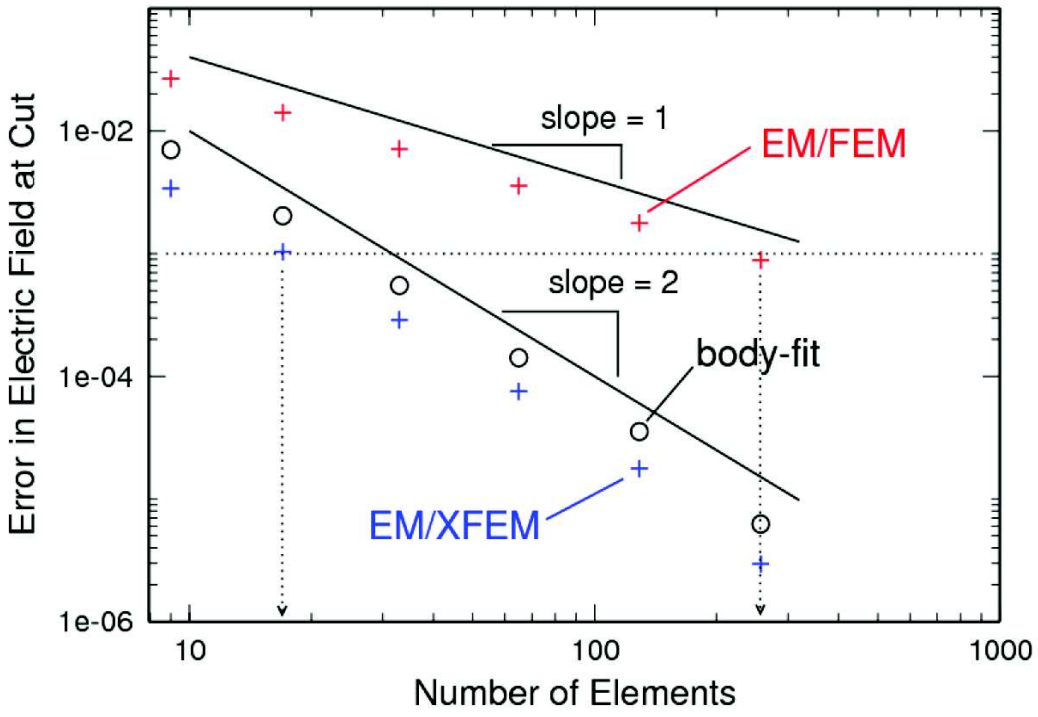

Figure 8: Error in cut-location electric field as a function of mesh refinement. Results are shown for EM/XFEM, body-fit EM/FEM and non-conforming EM/FEM. All results were produced using rectangular edge elements.

body-fit FEM in our example. There are numerous unanswered research questions involving the calculation of the electric field using EM-XFEM, including demonstrating this capability on more general 2D and 3D problems and dealing with so-called sliver cuts (cuts that are very close to the element boundary. Other research questions include the development of a scheme to allow EM-XFEM to provide divergence-free updates to the magnetic field (a key reason to use edge elements), developing a scalable solver for linear systems resulting from EM-XFEM and calculating derived quantities like the Lorentz force and Joule heating.

Acknowledgments

This work has been supported by the LDRD program at Sandia National Laboratories.

References

[1] A. Bedford and D. Drumheller. Theories of immiscible and structured mixtures. *Int. J. Engng. Sci.*, 21(8):863–960, 1983.

[2] D. Benson. Computational methods in lagrangian and eulerian hydrocodes. *Comput. Methods Appl. Mech. Engrg.*, 99:235–394, 1992.

[3] P. Bochev and M. Gunzburger. *Least-Squares Finite Element Methods*, volume 166 of *Applied Mathematical Sciences*. Springer, 2009.

[4] P. Bochev and J. Hyman. Principles of mimetic discretizations of differential operators. In D.N. Arnold, P.B. Bochev, R.B. Lehoucq, R.A. Nicolaides, and M. Shashkov, editors, *Compatible Spatial Discretizations*. Springer-Verlag, 2006.

[5] P. Bochev and A. Robinson. Matching algorithms with physics: exact sequences of finite element spaces. In D. Estep and S. Tavener, editors, *Preservation of stability under discretization*, pages 145–165, Philadelphia, 2001. SIAM.

[6] A. Bossavit. Whitney forms: A class of finite elements for three dimensional computations in electromagnetism. *IEEE Proceedings*, 135(8):493–500, 1988.

[7] J. Chessa and T. Belytschko. An extended finite element method for two-phase fluids. *Journal of Applied Mechanics*, 70:10–17, 2003.

[8] J. Dolbow, N. Moës, and T. Belytschko. Discontinuous enrichement in finite elements with a partition of unity method. *Finite Element Methods in Analysis and Design*, 36:235–260, 2000.

[9] R. Doney. ALEGRA simulations of magnetic flux compression using coaxial and helicoil conductors. In preparation.

[10] D. Drumheller. On theores for reactive immiscible mixtures. *Int. J. Engng. Sci.*, 38:347–382, 2000.

[11] A. Robinson et al. Alegra advanced/mhd training course. Technical Report SAND 2011-7643P, Sandia National Laboratories, October 2011.

[12] C. Fowler, S. Caird, and W. Garn. An introduction to explosive magnetic flux compression generators. Technical Report LA-5890-MS, Los Alamos National Laboratories, March 1975.

[13] J. Gyselinck and P. Dular. A time-domain homogenization technique for laminated iron cores in 3-d finite-element models. *IEEE Trans. Magn.*, 40(2):856–858, 2004.

[14] A. Hansbro and P. Hansbro. A finite element method for simulation of strong and weak discontinuities in solid mechanics. *Computer Methods in Applied Mechanics and Engineering*, 193:3523–3540, 2004.

[15] H. Ji, D. Chopp, and J. Dolbow. A hybrid extended finite element-level set model for modeling phase transformations. *International Journal for Numerical Methods in Engineering*, 54:1209–1233, 2002.

[16] J. Jin. *The finite element method in electromagnetics*. Wiley-Interscience, New York, second edition, 2002.

[17] F. Lefevre, S. Lohrengel, and S. Nicaise. An extended finite element method for 2d edge elements. *Int. J. Num. Anal. Modeling*, 8:641–666, 2011.

[18] R. Lemke, M. Knudson, D. Bliss, K. Cochrane, J.-P. Davis, A. Giunta, H. Harjes, and S. Slutz. Magnetically accelerated, ultrahigh velocity flyer plates for shock wave experiments. *J. Appl. Phys.*, 98, 073530, 2005.

[19] J.M. Melenk and I. Babuska. The partition of unity finite element method: basic theory and applications. *Computer Methods in Applied Mechanics and Engineering*, 139:289–314, 1996.

[20] N. Moes, J. Dolbow, and T. Belytschko. A finite element method for crack growth without remeshing. *Int. J. Numer. Meth. Engng.*, 46:131–150, 1999.

[21] J. Robbins and T. Voth. Modeling dislocations in a polycrystal using the generalised finite element method. *International Journal of Theoretical and Applied Multiscale Mechanics*, 2:95–110, 2011.

[22] A. Robinson, T. Brunner, S. Carrol, R. Drake, C. Garasi, T. Gardiner, H. Hanshaw, D. Hensinger, D. Labreche, R. Lemke, E. Love, C. Luchini, S. Mosso, J. Niederhaus, C. Ober, S. Petney, W. Rider, G. Scovazzi, O. Strack, R. Summers, T. Trucano, V. Weirs, M. Wong, and T. Voth. ALEGRA: an arbitrary Lagrangian-Eulerian multimaterial, multiphysics code. In *Proceedings of the 46th AIAA aerospaces sciences meeting*, 2008.

[23] J.-H. Song, P. Areias, and T. Belytschko. A method for dynamic crack and shear band propagation with phantom nodes. *International Journal for Numerical Methods in Engineering*, 67:868–893, 2006.

[24] E. Tuncer, Y. Serdyuk, and S. Gubanski. Dielectric mixtures: electrical properties and modeling. *IEEE Trans. Dielectr. Electr. Insul.*, 9(5):809–828, 2002.

[25] J. van Welij. Calculation of eddy currents in terms of H on hexahedra. *IEEE Trans. Magn.*, 21(6):2239–2241, 1985.

[26] T. Voth and S. Mosso. An eXtended Finite Element/Eulerian (XFEM/Eulerian) approach for solid mechanics. In *Proceedings of the 2012 Research in BAllistic Protection Technologies Conference*, Aberdeen Proving Ground, MD, 2012. ARL.

[27] H. Waki, H. Igarashi, and T. Honma. Analysis of magnetic shielding effect of layered shields based on homogenization. *IEEE Trans. Magn.*, 42(4):847–850, 2006.